ELSEVIER

Tectonophysics 303 (1999) 175–191

TECTONOPHYSICS

Frictional–viscous flow in mylonite with varied bimineralic composition and its effect on lithospheric strength

M.R. Handy *, S.B. Wissing, L.E. Streit [1]

Institut für Geowissenschaften, Universität Giessen, D-35390 Giessen, Germany

Received 1 August 1997; accepted 10 February 1998

Abstract

A theoretical, composite flow law is presented for mylonite containing interconnected layers of a weak mineral undergoing power law creep and porphyroclasts of a stronger mineral undergoing fracture and frictional sliding. Such mylonite, termed clastomylonite, is said to undergo frictional–viscous (FV) mylonitic flow. Its bulk strength is expressed as a function of bimineralic composition, temperature, effective pressure, and shear strain rate, as well as the material parameters for the constituent minerals. The FV flow law predicts that the rheology of clastomylonite is predominantly non-linear viscous and only slightly pressure-sensitive for most bimineralic compositions. FV mylonitic flow is shown to occupy a depth interval between cataclastic flow involving adhesive wear in the upper crust and fully viscous mylonitic flow at greater depths. The transition from adhesive wear to FV mylonitic flow is related to the onset of dislocation creep (glide-plus-climb) in the weakest phase and is inferred to coincide with a crustal strength maximum. A peak strength of about 80 MPa is calculated with a combination of Byerlee's constants for frictional sliding of granite and the FV flow law for granitic clastomylonite (30 vol.% quartz) at elevated fluid pressures. This value falls within the range of flow stresses independently obtained from quartz palaeopiezometry in many greenschist facies, granitic mylonite zones.

Keywords: brittle–ductile transition; polyphase rheology; mylonite

1. Introduction

Mylonite or mylonitic fault rock is generally considered to originate at crustal depths where deformation involves predominantly temperature- and strain-rate-dependent, intracrystalline plasticity (e.g., Sibson, 1977; Scholz, 1990 and references therein). Yet in most mylonite, the mineral or minerals making up the matrix usually deform by one or more thermally activated deformation mechanisms that are associated with both non-linear (dislocation creep) and linear (diffusion-accommodated grain-boundary sliding, pressure solution) viscous rheologies (Schmid and Handy, 1990). Deformation involving such mechanisms is therefore termed viscous flow. The inclusions within the mylonitic matrix deform either by viscous flow or cataclasis (e.g., Mitra, 1978; White et al., 1980). Handy (1990) therefore distinguished three types of steady-state microstruc-

* Corresponding author. Fax: +49-641-99-36019; E-mail: mark.handy@geo.uni-giessen.de
[1] Present address: Dept. of Geology, Australian National University, Australia.

0040-1951/99/$ – see front matter
PII: S0040-1951(98)00251-0

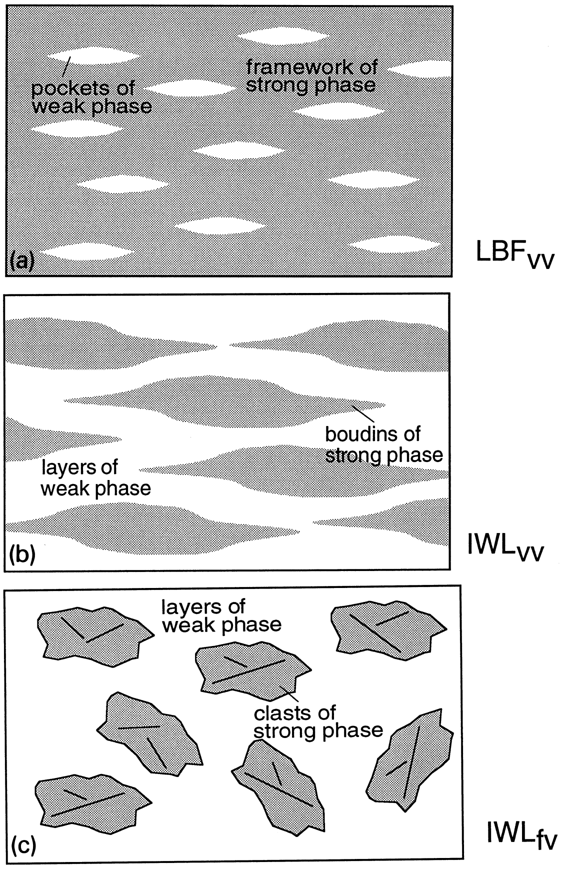

Fig. 1. Sketch of the three end-member types of steady-state, mylonitic microstructure modelled in this paper. (a) Mylonite with both minerals deforming viscously and the strong mineral forming a load-bearing framework. (b) Mylonite with both minerals deforming viscously and the weaker mineral forming interconnected layers. (c) Mylonite with weak, viscous mineral in interconnected layers and stronger porphyroclasts deforming cataclastically. *LBF* = load-bearing framework; *IWL* = interconnected weak layers. Subscripts denote rheologies (f = frictional, v = viscous) of the strong and weak minerals in the rock. See text for definitions.

ture in mylonite on the basis of the shape, distribution and contrasting rheologies of their constituent minerals. The first type is a load-bearing framework (LBF) structure (Fig. 1a), whereas the second and third types have an interconnected weak layer (IWL) structure containing viscous boudins (Fig. 1b, IWL$_{vv}$) or porphyroclasts (Fig. 1c, IWL$_{fv}$). The subscripts refer to the general rheology (f = frictional, v = viscous) of the strong and weak minerals in the rock.

This paper focusses on the rheology of mylonite in which interconnected layers of a weak mineral deform by viscous flow and porphyroclasts of a strong mineral undergo frictional flow, i.e., cataclasis (microcracking, frictional sliding, and rigid-body rotation), as depicted in Fig. 1c. We refer to such a mylonite as 'clastomylonite', to its microstructure as IWL$_{fv}$, and to the bulk deformation of its structurally segregated minerals as frictional–viscous or 'FV mylonitic flow'. Because porphyroclasts undergo cataclasis and cataclasis involves dilatancy, one can predict that the bulk deformation of clastomylonite has a dilatant component and is therefore pressure- as well as temperature- and strain-rate-dependent. Such mixed P-, T- and $\dot{\varepsilon}$-dependent behaviour is often termed 'semi-brittle' (Carter and Kirby, 1978) or 'quasi-plastic' (Sibson, 1977; Sibson, 1986) in the rock mechanics literature. We will avoid these terms, however, because 'quasi-plastic' connotes intracrystalline plasticity (Sibson, 1977) and apparently excludes other viscous flow mechanisms such as diffusion creep, whereas 'semi-brittle' is often also used in a mechanistic sense to describe distributed microcracking and frictional grain-boundary sliding (cataclasis) with adhesive wear along sliding surfaces (Scholz, 1988; Evans and Kohlstedt, 1995). Adhesive wear involves limited intracrystalline plasticity and is inferred to occur within a specific depth-range of the crust between fully frictional, abrasive wear and fully viscous flow (Scholz, 1988; Scholz, 1990). As discussed in the last part of this paper, the rheology and microstructure of a cataclasite undergoing adhesive wear are probably quite different than those of clastomylonite undergoing FV mylonitic flow.

In recent years, several approaches have been developed to model heterogeneous viscous flow of coarse-grained, polyphase rock. Tullis et al. (1991) digitized both the microstructure of real rock and the geometry of idealized inclusions as a basis for finite element modelling of aggregate viscous strength. Although refined, this method is so rock-specific and time-intensive as to be of limited practical use in modelling lithospheric rheology. Based on their calculated finite-element rock strengths, these authors derived a set of empirical equations expressing the non-linear dependence of material parameters on composition for power law creep. However, their approach is only valid when applied to rocks whose constituent minerals have low viscous strength contrasts (Tullis et al., 1991). Handy (1994a) derived composite flow laws for mylonite containing two viscous phases and having either LBF_{vv}, or IWL_{vv} microstructures (Fig. 1a,b); the IWL_{fv} microstructure was neglected. Ji and Zhao (1993) presented an iterative function for averaging uniform strain rate and uniform stress estimates of viscous aggregate strength with an arbitrary number of phases. As in older models based on similar principles (e.g., Voight–Hill–Reuss), the physical significance of the averaging procedure is unclear. In another attempt, Ji and Zhao (1994) modified elasto-plastic fibre-loading theory to obtain visco-plastic flow equations for clastomylonitic aggregates. Unfortunately, composite strength in these equations is not an explicit function of pressure and temperature. Ivins and Sammis (1996) adopt Maxwellian visco-elastic rheologies for weak spherical inclusions in a strong matrix (LBF_{vv} structure) to model transient, composite creep of the lower crust.

Clearly, existing models for the composite rheology of rocks simulate some, but not all of the main features of mylonitic deformation. Either these models do not explicitly incorporate realistic mylonitic microstructures, or they neglect the bulk rheological effects of P-dependent, brittle behaviour in one of the mineral phases and T- and $\dot{\varepsilon}$-dependent behaviour in the other.

In this paper, we extend the phenomenological approach of Handy (1994a) to develop a new composite flow law for clastomylonite. We then employ a criterion of strain energy minimization to determine the dynamic stability of the IWL_{fv} microstructure in clastomylonite relative to that of the LBF_{vv} and IWL_{vv} microstructures in mylonites whose constituent minerals undergo viscous, power law creep. The new composite flow law is used to constrain the compositional dependence of lithospheric strength and to predict the strength of natural quartzofeldspathic mylonite. Various material parameters for failure and frictional sliding are substituted into the new flow law to examine the effect of different local stress states on the potential depth-range of porphyroclast formation. Finally, we cast the results of our modelling in a more general context to modify current notions on the relationship between rock structure and lithospheric rheology.

2. Theory

The general approach adopted below to predict the strength and structure of bimineralic mylonite involves two steps (Handy, 1994a). First, we derive flow laws for mylonite with the three steady-state microstructures depicted in Fig. 1. We then employ a criterion of strain energy minimization for determining which of these microstructures is stable at a specified set of conditions.

2.1. Flow laws for fully viscous mylonites (LBF_{vv} and IWL_{vv} microstructures)

Mylonite with an LBF_{vv} microstructure has a viscously deforming framework of strong mineral containing inclusions of a weaker, viscously deforming mineral (Fig. 1a). The strong, load-bearing framework constrains the weaker inclusions to deform at the same rate, leading to a uniform strain rate, upper bound approximation of composite viscous shear strength, τ_r^{LBF}:

$$\tau_r^{LBF} = \tau_{wr}\phi_w + \tau_{sr}(1 - \phi_w) \tag{1}$$

where the superscript LBF denotes the load-bearing framework structure and the subscript r indicates the composite rock. τ_{wr} and are τ_{sr}, the shear strengths of the weak and strong phases. The subscripts wr and sr indicate that the shear strengths of the constituent phases are defined at a reference shear strain rate equal to the shear strain rate of the entire rock ($\dot{\gamma}_r$). ϕ_w is the volume proportion of weak phase in the rock. Note that in a bimineralic rock, $(1 - \phi_w) = \phi_s$, where ϕ_s is the volume proportion of strong phase. Only steady-state microstructures are considered in this paper, so the volume proportions of both phases remain constant with strain.

Both the weak and strong minerals are assumed to deform solely by dislocation creep and therefore to have rheologies that obey the empirically derived power law for thermally activated creep (Weertman, 1968):

$$\tau = \exp\left\{\frac{1}{n}\left[\frac{Q}{RT} + \ln\left(\frac{\dot{\gamma}}{3^{(n+1)/2}A}\right)\right]\right\} \tag{2}$$

where τ and $\dot{\gamma}$ represent the shear strength and shear strain rate in a mineral phase at temperature T, and where the material constants are the activation enthalpy of creep Q, the creep exponent n, and the pre-exponential function A. The factor $3^{(n+1)/2}$ (Nye, 1953) converts the stress and strain rate tensors of the flattening configuration in the triaxial experiments to the octahedral shear configuration used to approximate simple shear. We note that the stresses and strain rates of the constituent minerals are not specified at every point within the aggregate and therefore represent only averages of the actual heterogeneous stresses and shear strain rates. In real rocks, both stress and strain rate vary within the microstructure, depending on the shape, distribution and relative proportions of minerals with contrasting rheologies (see fig. 6 in Handy, 1990; figs. 4 and 7 in Tullis et al., 1991). The effects on composite rock strength of averaging stress and strain rate are discussed on pp. 299–300 of Handy (1994a).

Mylonites with IWL structures comprise interconnected layers of weak phase that surround either viscously deforming boudins (Fig. 1b) or brittly deforming inclusions (Fig. 1c) of a stronger phase. The interconnectedness of the weak layers allows them to accommodate an amount of shear strain that is inversely and non-linearly proportional to both the volume proportions and the viscous strength contrast τ_c of the constituent minerals. The relationship between the shear strain rates of the weak and strong phases in the rock (respectively $\dot{\gamma}_w$ and $\dot{\gamma}_s$) and the bulk shear strain rate of the rock, $\dot{\gamma}_r$, is (full derivation on pp. 295–296 in Handy, 1994a; see Handy, 1994b for a minor correction):

$$\dot{\gamma}_w = \dot{\gamma}_r \phi_w^{-1/\tau_c} \tag{3}$$

$$\dot{\gamma}_s = \dot{\gamma}_r \frac{1 - \phi_w^{1-(1/\tau_c)}}{1 - \phi_w} \tag{4}$$

The viscous strength contrast τ_c is defined as the ratio τ_{sr}/τ_{wr}, where τ_{wr} and τ_{sr} are the reference shear strengths of the weak and strong phases, as defined above in Eq. 1. The shear strength of a mylonite with an IWL microstructure, τ_r^{IWL}, is then:

$$\tau_r^{IWL} = \tau_w \phi_w^{-1/\tau_c} + \tau_s \left(1 - \phi_w^{-1/\tau_c}\right) \tag{5}$$

where τ_w and τ_s are the shear strengths of the weak and strong phases deforming, respectively, at the shear strain rates $\dot{\gamma}_w$ and $\dot{\gamma}_s$ in Eqs. 3 and 4 for a specified volume proportion of weak phase ϕ_w.

Substituting Eq. 2 and the appropriate material constants therein into the τ_{wr} and τ_{sr} terms in Eq. 1 allows one to calculate the shear strength of mylonite with the LBF_{vv} microstructure. Likewise, substitution of Eq. 2 and the material constants of the constituent minerals into the τ_w and τ_s terms in Eq. 5 allows one to calculate the shear strength of mylonite with the IWL_{vv} microstructure. In both cases, one must specify the volume proportion of weak phase ϕ_w, the temperature T, and the bulk rock strain rate $\dot{\gamma}_r$.

2.2. Flow law for clastomylonite (IWL_{fv} microstructure)

Up to this point, we have followed closely Handy's (1994a) derivation for the rheologies of fully viscous mylonites with LBF_{vv}, and IWL_{vv} microstructures. We now modify this theory to derive a constitutive equation for clastomylonite undergoing FV mylonitic flow (Fig. 1c). In clastomylonite, the weak phase is assumed, as above, to deform by dislocation creep (Eq. 2), but the shear strength of the strong phase (porphyroclasts) is obtained from the modified Navier–Coulomb criterion for frictional sliding (Jaeger and Cook, 1979; Streit, 1997):

$$\tau_s = \tfrac{1}{2}\left[a + P_{eff}(b-1)\right] \sin(90 - \arctan \mu_d) \tag{6}$$

where the effective pressure, $P_{eff} = P_{lith} - P_{pore}$ (respectively the lithostatic and pore fluid pressures), and where $a = 2\tau_o\sqrt{b}$ and $b = \left[(1+\mu_d^2)^{0.5} - \mu_d\right]^{-2}$. The coefficient of dynamic friction, $\mu_d = 0.6$, and the critical shear strength, $\tau_o = 50$ MPa, are taken from Byerlee (1978) and are assumed not to vary with temperature and effective pressure over the range of depths considered below (Stesky et al., 1974).

Note that in using Eq. 6 to simulate frictional sliding, we tacitly stipulate a compressive stress state within the porphyroclasts, such that the effective pressure P_{eff} is set equal to the effective, intermediate and least principal stresses, $\sigma_2 = \sigma_3$. Used together with the Byerlee (1978) constants, this criterion also implies that the sliding microfault surfaces within the porphyroclasts maintain an optimum angle of 30° to the σ_1 direction in the mylonite. In simple shear, σ_1 is oriented at 45° to the shear zone boundaries and these microfaults are therefore inclined at a low angle (15°) to the mylonitic foliation. This orientation is quite reasonable for frictional sliding on ideally irrotational surfaces in clasts at moderate to high shear strains, but obviously does not represent the attitudes of all rotated sliding surfaces or of purely extensional cracks at high angles to the mylonitic foliation. For the sake of simplicity, we will neglect the effect of unfavourably oriented, rotating sliding surfaces on porphyroclast strength. This effect is probably small compared to some of the weakening factors (pre-existing anisotropies, fluid pressure, subcritical cracking) discussed below.

To obtain the full expression for the shear strength of a clastomylonite, one first substitutes Eq. 2 and the creep parameters of the weak mineral into the τ_{wr} term in Eq. 5 and then substitutes Eq. 6 and the frictional constants for the strong mineral into the τ_s term in Eq. 5. In the resulting new expression, the shear strength of the bimineralic rock depends not only on T, $\dot{\gamma}_r$, and ϕ_w, but also on effective pressure P_{eff}, as expected for a rock containing inclusions that dilate.

2.3. A criterion for the stability of steady state microstructures in polyphase rocks

Having derived expressions for all of the mylonitic microstructures depicted in Fig. 1, we now propose a criterion which allows us to determine the relative stability of the LBF_{vv}, IWL_{vv}, and IWL_{fv} microstructures at given values of effective pressure, temperature, bulk strain rate and volume proportions of the constituent minerals. We shall assume that strain energy is minimized in deforming aggregates and therefore that the most stable microstructure dissipates the least amount of strain energy per unit time and per unit volume of rock (Handy, 1994a). The rate of strain energy dissipation for a unit volume of bimineralic rock $\dot{E}_r$, is given by the relation $\dot{E}_r = \tau_w \dot{\gamma}_w \phi_w + \tau_s \dot{\gamma}_s \phi_s$, where all other terms have been defined above. In Fig. 2, for example, $\dot{E}_r$ is plotted as a function of ϕ_w for different microstructures and flow mechanisms at given values of effective pressure, temperature, and bulk strain rate. The low position of the energy dissipation rate curve for the IWL_{fv} microstructure on the left-hand side of the diagram indicates that this microstructure is more stable at low ϕ_w values, whereas the IWL_{vv} microstructure predominates at intermediate and high ϕ_w values. The LBF_{vv} microstructure yields higher $\dot{E}_r$ values and is therefore unstable with respect to the other two mylonitic microstructures at all bimineralic compositions. The horizontal curves for cohesionless and cohesive frictional sliding at the top of the diagram were calculated with the Navier–Coulomb relation in Eq. 6 and are therefore independent of ϕ_w. Frictional sliding yields the highest $\dot{E}_r$ values for all ϕ_w values and so cataclastic microstructures are less stable than any of the mylonitic microstructures at the hypothetical conditions of deformation in Fig. 2.

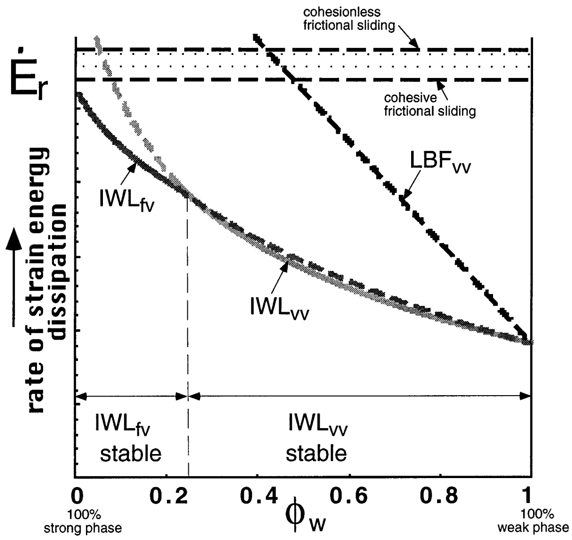

Fig. 2. Rate of strain energy dissipation of the composite rock E_r, versus volume proportion of weak mineral ϕ_w. Generic $\dot{E}_r$ curves for mylonites with LBF_{vv}, IWL_{vv}, and IWL_{fv} microstructures (see Fig. 1), and for cataclasites undergoing cohesive and cohesionless frictional sliding. Vertical dashed line delimits low ϕ_w range in which mylonite with IWL_{fv} microstructure is energetically stabler from higher ϕ_w range in which mylonite with IWL_{vv}, is favoured.

Of course, the use of different material constants to calculate $\dot{E}_r$ would change the shapes and relative positions of the curves in Fig. 2 and yield differently configured microstructural stability fields (see next section, Fig. 3). Different configurations would also result if we derived flow laws for bimineralic rocks with three additional microstructures: (1) weak interconnected layers undergoing frictional flow around stronger, viscous inclusions; (2) a load-bearing framework undergoing frictional flow around weak, viscous inclusions; and (3) a load-bearing framework deforming viscously and containing weaker inclusions that undergo frictional flow. None of these microstructures were considered here, partly because they have never been recognized in naturally deformed rocks (to our knowledge at least), and also because of the special, possibly transient conditions that may favour their potential occurrence in the lithosphere. For example, a frictionally flowing framework containing weak, viscous inclusions may only exist in rocks that deform at low effective pressures (i.e., low lithostatic pressures and/or high pore fluid pressures) and whose inclusions have low activation enthalpies for creep (e.g., halite inclusions in anhydrite). Simulating such behaviour lies beyond the scope of this paper and may be considered sometime later.

We conclude this section by emphasizing that composite shear strengths obtained with the flow laws above are only as good as the quality of the experimentally determined parameters used in these flow laws. As the use of these parameters in extrapolating flow laws from experimental to natural strain rates is problematic (Paterson, 1987), the estimates of mylonitic strength obtained with the equations above should only be interpreted qualitatively.

3. Applications

3.1. Strength of the lithosphere

The flow laws derived above can be used to calculate lithospheric strength as a function of both depth and bimineralic composition for mylonites with the LBF_{vv}, IWL_{vv}, and IWL_{fv} microstructures. Fig. 3a contains shear strength versus depth profiles for horizontally foliated sections of continental lithosphere comprising granite (30% quartz, 70% feldspar), gabbro (30% feldspar, 70% clinopyroxene), and lherzolite (50% olivine, 50% pyroxene), all deforming at a bulk shear strain rate of $\dot{\gamma}_r = 10^{-12}$ s^{-1}, a geothermal gradient of 20ºC/km, and a geobaric gradient of 27.5 MPa/km. For each of these lithological sections, shear strength versus composition diagrams calculated for the same $\dot{\gamma}_r$, and for given lithostatic pressures and temperatures are shown in Fig. 3b. The lithostatic pressures and temperatures for these diagrams correspond to depths within a hypothetical lithospheric column that are marked with arrows on the vertical axes of the adjacent shear strength versus depth profiles in Fig. 3a. To keep matters relatively simple, we have assumed zero pore fluid pressure (see discussion below).

Before we explore the implications of Fig. 3, a clarifying word about the construction and interpretation of the diagrams is necessary. In Fig. 3a, each shear strength versus depth profile includes strength curves for the following flow mechanisms (see caption for material parameters): (1) stable, cohesionless frictional flow; (2) stable, cohesive frictional flow; (3) FV mylonitic flow (IWL_{fv} microstructure); and (4) fully viscous flow for mylonite with an IWL_{vv} microstructure. The intersections of these strength curves delimit differently patterned depth intervals (separated by horizontal, dashed lines) corresponding to domains of different microstructural stability (see legend in Fig. 3). Within each of these depth intervals, only one steady-state microstructure is pre-

Fig. 3. Bulk shear strength versus depth profiles (a) and bulk shear strength versus composition diagrams (b) for different bimineral rocks with LBF_{vv}, IWL_{vv}, and IWL_{fv} microstructures in the continental lithosphere. Dashed lines in (a) and (b) delimit microstructural stability fields indicated by different patterns (see legend). Solid curves in (a) are shear strength curves for rocks with energetically stable microstructures, whereas dotted parts of these curves indicate shear strength at conditions for which the same microstructures are energetically unstable (see text for explanation). Arrows on the vertical axes in (a) indicate depths corresponding to lithostatic pressures and temperatures in adjacent diagrams in (b), whereas dots in (b) indicate composition and shear strength at the shear strain rate of the adjacent profiles in (a). Microstructural stability fields in (b) are contoured for shear strength (solid curves) at shear strain rate increments of a half an order of magnitude. Shear strength contrasts τ_c, of the minerals at selected bulk shear strain rates are included along the right-hand vertical axes of the diagrams. Profiles and diagrams constructed with equations discussed in text and the flow laws of Jaoul et al. (1984) for quartzite ($n = 2.4$, $Q = 163$ kJ/m, $A = 10^{-5}$ MPa-n/s), Shelton and Tullis (1981) for albitic feldspar rock ($n = 3.9$, $Q = 234$ kJ/m, $A = 2.51 \times 10^{-6}$ MPa-n/s), Boland and Tullis (1986) for clinopyroxenite ($n = 3.3$, $Q = 490$ kJ/m, $A = 10^{5.17}$ MPa-n/s), Chopra and Paterson (1981) for dunite ($n = 3.35$, $Q = 444$ kJ/m, $A = 9.55 \times 10^3$ MPa-n/s), Byerlee (1978) for cohesionless ($\mu_d = 0.85$, $\tau_o = 0$) and cohesive ($\mu_d = 0.6$, $\tau_o = 50$ MPa) frictional sliding. Conditions assumed: geothermal gradient, $T' = 20$ºC/km, bulk shear strain rate $\dot{\gamma}_r = 10^{-12}$ s^{-1}, pore fluid pressure is zero, geobaric gradient is 27.5 MPa/km for an average crustal density of 2.8 g/cm3.

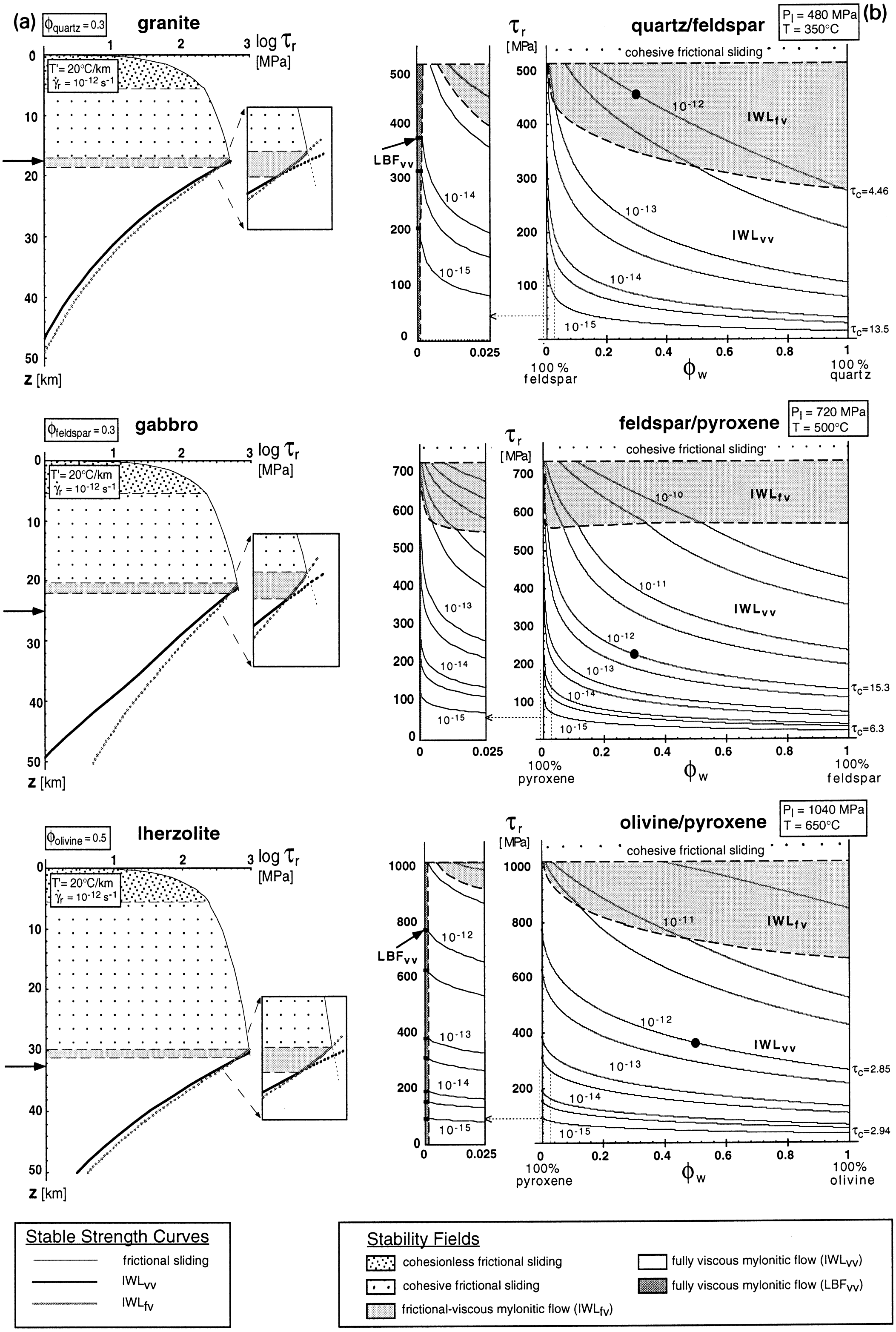
(a)
granite
gabbro
lherzolite
log τr [MPa]
z [km]
T' = 20°C/km
(b)
quartz/feldspar
P_l = 480 MPa
T = 350°C
feldspar/pyroxene
P_l = 720 MPa
T = 500°C
olivine/pyroxene
P_l = 1040 MPa
T = 650°C
cohesive frictional sliding
IWL_fv
IWL_vv
LBF_vv
τr [MPa]
φw
100 % feldspar
100 % quartz
100% pyroxene
100% feldspar
100% olivine
τc=4.46
τc=13.5
τc=15.3
τc=6.3
τc=2.85
τc=2.94
Stable Strength Curves
frictional sliding
IWL_vv
IWL_fv
Stability Fields
cohesionless frictional sliding
cohesive frictional sliding
frictional-viscous mylonitic flow (IWL_fv)
fully viscous mylonitic flow (IWL_vv)
fully viscous mylonitic flow (LBF_vv)

dicted to be stable, namely, that microstructure with the lowest rate of strain energy dissipation for the given conditions of deformation. The strain energy dissipation rates of the microstructures can be inferred directly from the relative positions of the shear strength curves in Fig. 3a because bulk shear strength is proportional to energy dissipation rate per unit volume of rock at constant bulk strain rate ($\tau_r = \dot{E}_r/\dot{\gamma}_r$, recall that the profiles in Fig. 3a are valid for constant shear strain rate and mineral volume proportions). The dotted segments of the shear strength curves in Fig. 3a indicate the depth intervals over which the microstructures are energetically unstable (or metastable at low shear strains) according to the stability criterion above. Shear strength curves for mylonite with the LBF_{vv} microstructure were not included in Fig. 3a because this microstructure dissipates strain energy at a higher rate and is therefore energetically unstable with respect to the other microstructures for the bimineralic compositions and depth range considered here. The criterion of strain energy minimization was also used to construct the shear strength versus composition diagrams in Fig. 3b. In contrast to the profiles in Fig. 3a, however, these diagrams show stability fields for the aforementioned microstructures over the entire range of bimineralic compositions. In addition, each field contains bulk shear strength contours for different values of the bulk shear strain rate $\dot{\gamma}_r$. The dashed boundaries between microstructural stability fields within the diagrams in Fig. 3b are analogous to the horizontal dashed lines in Fig. 3a that separate depth intervals containing different, stable, steady-state microstructures.

The stability fields for the IWL_{vv}, and IWL_{fv} microstructures cover most of the diagrams in Fig. 3b. The LBF_{vv} field is restricted to a small range of low ϕ_w values on the left side of the diagram for quartz–feldspar and olivine–pyroxene rocks, and is not present at all in the diagram for feldspar–pyroxene rock (insets of diagrams in Fig. 3b). In general, the IWL_{fv}, microstructure is favoured at high bulk strain rates and/or low temperatures, corresponding to high mineral strength contrasts. The asymmetrical, concave shape of the strength contours in both IWL stability fields indicates that rock strength is most dependent on bimineralic composition at low ϕ_w values. Thus, only a modest amount of weak mineral in interconnected layers parallel to the shearing plane suffices to reduce the bulk strength of the rock to levels approaching that of the pure weak mineral.

The pressure-dependence of FV flow in clastomylonite (IWL_{fv} microstructure) increases nonlinearly with decreasing temperature (Fig. 4a) and with increasing volume proportion of porphyroclasts (Fig. 4b). At high temperatures and/or high volume proportions of interconnected weak phase, the T and

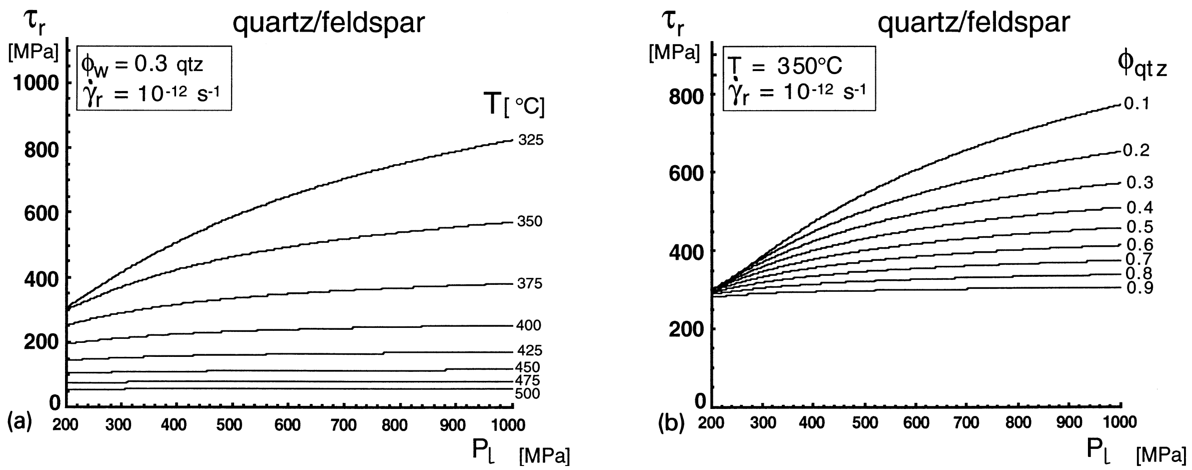

Fig. 4. Pressure dependence of FV mylonitic flow in quartz–feldspar clastomylonite: (a) shear strength versus lithostatic pressure diagram with shear strength curves for different temperatures T, at constant shear strain rate ($\dot{\gamma}_r = 10^{-12}$ s^{-1}) and volume proportion of weak phase ($\phi_w = 0.3$ quartz); (b) shear strength versus lithostatic pressure diagram with shear strength curves for different volume proportions ϕ_w quartz, at constant $\dot{\gamma}_r$ (10^{-12} s^{-1}) and T (350°C).

ϕ_w contours are nearly flat (Fig. 4), indicating that the temperature-dependence of FV mylonitic flow is similar to that of fully viscous mylonitic flow in an IWL_{vv} microstructure.

In the shear strength versus depth profiles in Fig. 3a, the IWL_{fv} microstructure is stable over a relatively narrow depth interval between frictional flow in the upper crust and fully viscous flow at greater depths. We found that this prediction holds for any combination of experimental monomineralic flow laws currently available in the literature for the minerals making up the bimineralic rock. In nature, however, the actual depth range of FV mylonitic flow is probably much larger due to several phenomena that, acting individually or in concert, can weaken the porphyroclasts:

(1) Pressurized metamorphic fluids reduce effective pressure and, in triaxial rock deformation experiments, have been shown to decrease rock strength and induce fracture (e.g., Handin et al., 1963; Murrel, 1965; Paterson, 1978). Healed syn-mylonitic microveins containing hydrous minerals within competent inclusions (Fig. 5) are testimony to fracturing in the presence of pressurized fluids in high-grade shear zones. The feldspar inclusions in Fig. 5 are elongate and show no evidence (e.g, asymmetrical tails, arcuate inclusion trails) of having rotated in the surrounding matrix during mylonitic deformation. Therefore, the moderate angle of these microveins with respect to the mylonitic foliation (Fig. 5) is probably primary and suggests that they initiated oblique to the shearing plane as purely extensional or as hybrid extensional-shear fractures, possibly along pre-existing twinning planes. This vein geometry also indicates that fluid pressures were close to the magnitude of the minimum principal stress and that the differential stresses in the porphyroclast were smaller than those required for compressional shear failure (Secor, 1965; Sibson, 1981; Etheridge, 1983).

(2) Subcritical crack growth within porphyroclasts can lead to a significant reduction in their long-term strength (Atkinson and Meridith, 1987). This type of crack propagation is associated with enhanced ionization and reaction rates in stressed regions around crack tips, leading to slow, stable growth of fractures at relatively low, local stress concentrations. Mitra (1984) inferred subcritical cracking from the termination of cracks at the clast-matrix interface and from the preservation of crack tips in clasts within mylonites (see his fig. 5). Existing experimental data indicate that subcritical crack growth is likely to occur over a broad range of temperatures, pressures, and fluid activities (Atkinson, 1984; Atkinson and Meridith, 1987). Unfortunately, subcritical crack propagation is still poorly understood and the limited data in the literature do not allow one to quantify its weakening effect on clastomylonites.

(3) Anisotropies within porphyroclasts (e.g., pre-existing fractures, cleavage or twinning planes) represent potential planes of weakness which, if oriented at low to moderate angles to the local direction of maximum principal stress σ_1, can be easily activated as sliding surfaces. Any of these effects would be expected to extend the depth range of FV mylonitic flow downwards at the expense of fully viscous flow.

To explore the weakening effect of pore fluid on the transition from frictional flow to FV mylonitic flow, we consider three end-member cases, corresponding to the three crustal strength curves for granitic rock (30% quartz, 70% feldspar) in Fig. 6. Case 1 is the reference state used in Figs. 3 and 4 above in which Byerlee's (1978) frictional constants for cohesionless ($\mu_d = 0.85$) and cohesive ($\tau_o = 50$ MPa, $\mu_d = 0.6$) frictional sliding are applied and the pore fluid factor, λ_v ($= P_{pore}/P_{lith}$) is assumed to be zero. In case 2, we again use Byerlee's frictional constants, but assume that near-lithostatic fluid pressures ($\lambda_v = 0.9$) prevail during cohesive frictional sliding at depths exceeding several kilometres. This is qualitatively consistent with the inferred build-up of supra-hydrostatic fluid pressures in shallow to intermediate parts of faults at several kilometres depth (Sibson, 1994; Streit, 1997). Streit and Cox (1998) have also shown that near-lithostatic fluid pressures existed at least transiently during mylonitization in some greenschist facies granitoid shear zones. Case 3 incorporates near lithostatic fluid pressure and a frictional coefficient of 0.6, but uses an average laboratory value of the cohesive shear strength ($\tau_o = 20$ MPa) for intact granites and gneisses (Handin, 1966) at elevated pressure instead of Byerlee's best-fit value of 50 MPa for a broad range of rock types. Stesky et al. (1974) have shown that a frictional coefficient of about 0.6 is valid for most basement

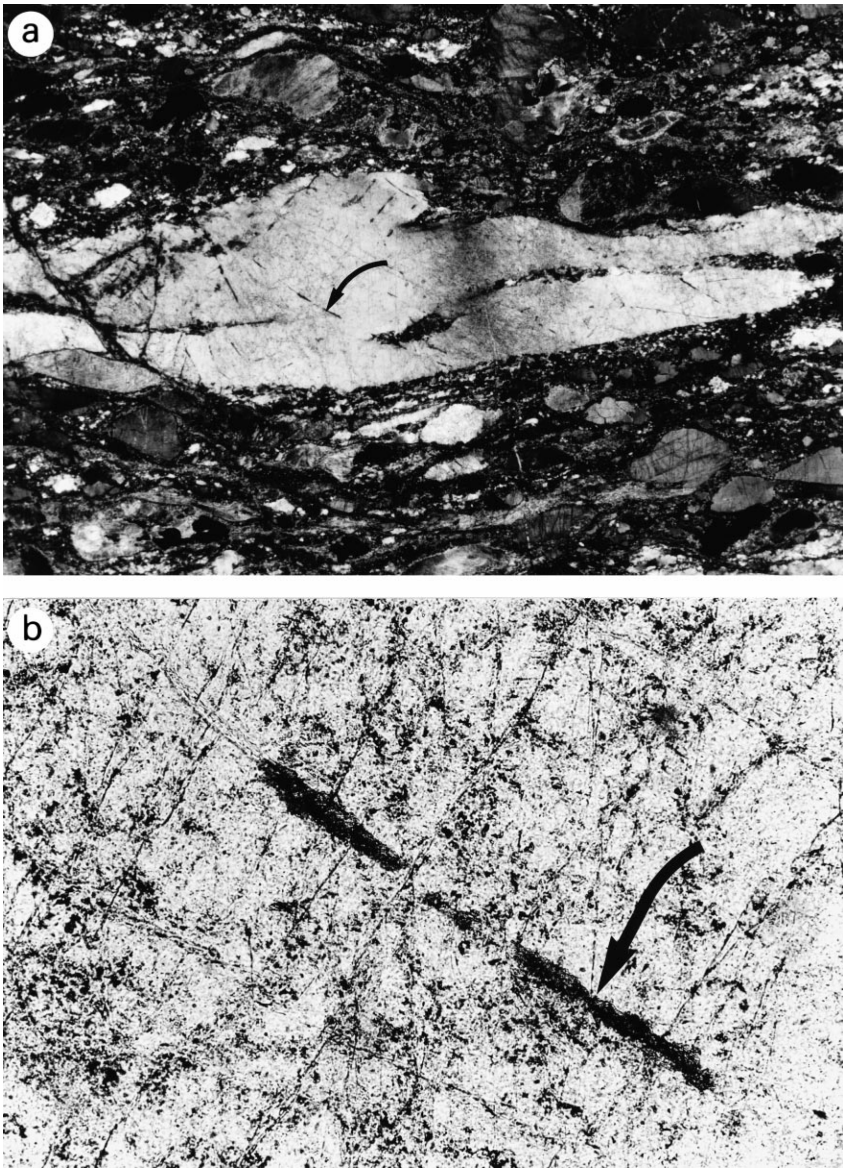

Fig. 5. (a) Mylonite with an IWL structure comprising competent inclusions of partly dynamically recrystallized, anorthitic feldspar in a weak matrix of dynamically recrystallized hornblende and brittly deformed clinopyroxene. Arrow within feldspar inclusion points to microvein shown in (b) (photo length 105 mm). (b) Close-up of partly healed, hornblende-filled microvein (arrow) in feldspar inclusion (see text for explanation). Narrowly spaced fractures offsetting this microvein formed during post-mylonitic cataclasis and are not relevant to this paper. Photo length 0.95 mm, sample Iv-850 from the Cannobina valley in the Ivrea–Verbano zone, northern Italy. Both pictures taken with crossed nichols. Thin section cut parallel to XZ fabric plane.

rocks at temperatures and normal stresses up to 600ºC and 600 MPa, respectively.

Fig. 6 shows that at high fluid pressure ($\lambda_v = 0.9$), FV mylonitic flow occurs within a somewhat broader depth range and at greater depths than in the absence of fluid pressure (compare curve 1 with curves 2 and 3, Fig. 6). Also at high fluid pressure, the transition between cohesive frictional sliding or fracturing of intact rock and FV mylonitic flow is shifted to lower depths. Not surprisingly, case 3

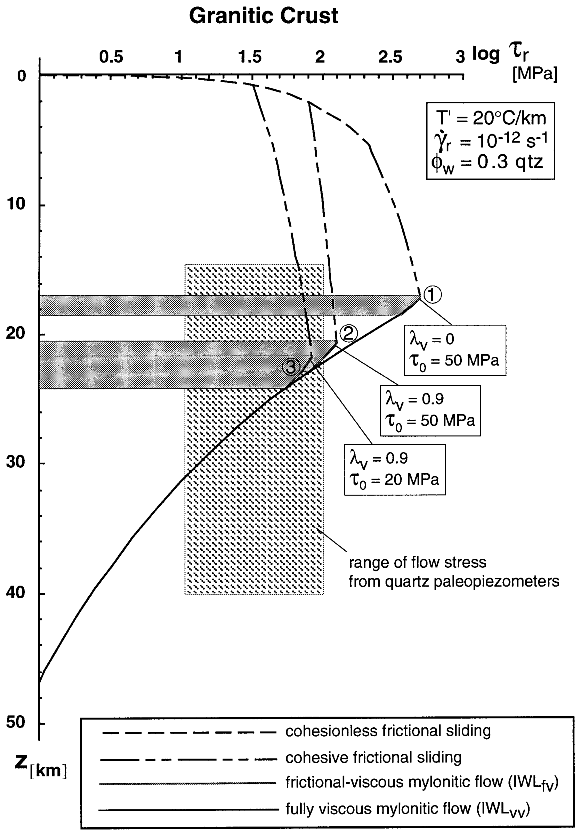

Fig. 6. Shear strength versus depth curves for granitic crust (30% quartz, 70% feldspar). Only energetically stable parts of the shear strength curves are shown. Numbers *1* to *3* refer to end-member cases incorporating different pore fluid factors and frictional constants in Eq. 6 for cohesive frictional sliding and for frictional flow of the porphyroclasts in clastomylonite, as discussed in text. Shaded horizontal bars indicate predicted depth range of FV mylonitic flow for each of these three cases. Rectangular patterned field represents range of flow stresses obtained from palaeopiezometry on dynamically recrystallized grains and subgrains of quartz in mylonite zones originating at different depths and temperatures (Kohlstedt and Weathers, 1980; Etheridge and Wilkie, 1981; Ord and Christie, 1984). Shear strength curves constructed with equations discussed in text and the flow laws of Jaoul et al. (1984) for quartzite, Shelton and Tullis (1981) for albitic feldspar rock, and Byerlee's (1978) constants for cohesionless and cohesive frictional sliding (parameters listed in caption to Fig. 3).

yields the lowest crustal shear strengths (curve 3 in Fig. 6). The estimated peak strength of about 80 MPa at the transition between cohesive frictional sliding and FV mylonitic flow for thrusting in case 3 is similar to the peak shear strength at the base of the seismogenic zone inferred for active faults at high fluid pressures (Streit, 1997) and falls within the range of flow stresses obtained independently from quartz palaeopiezometry in many crustal mylonite zones (shaded box in Fig. 6). This is consistent with the idea that brittle deformation within and immediately above the depth level for FV mylonitic flow occurs at transiently high pore fluid pressures ($\lambda_v = 0.9$). Substituting yet higher values of λ_v and/or lower values of μ_d into Eq. 6 in the flow law for clastomylonite dramatically extends the depth range of FV mylonitic flow and lowers the depth of the transition from cohesive frictional sliding to FV mylonitic flow.

3.2. Strength of natural mylonite

The bimineralic flow laws presented above can also be used to constrain the bulk strength of natural mylonites. To do this, one needs to know the range of temperatures and strain rates of deformation, and the volume proportions of the two minerals that accommodated most of the strain in the mylonite. Also, the mylonitic microstructure observed in nature should match one of the three, aforementioned model structures. Provided the minerals in the natural mylonite show evidence of deformation mainly by dislocation creep (in the matrix and/or clasts) or cataclasis (in the clasts), one can then estimate a range of bulk shear strengths.

For example, the quartz–feldspar clastomylonite in Fig. 7 contains feldspar clasts and interconnected layers of dynamically recrystallized quartz that define the mylonitic foliation. Quartz is inferred to have been the weaker phase at the time of deformation because it underwent dynamic recrystallization and because the feldspar clasts are fractured (Fig. 7a). The conditions of deformation are estimated to have been $T = 350$ to 400°C, $P = 480$ to 550 MPa at shear strain rates ranging from 10^{-11} to 10^{-13} s^{-1} (Handy, 1987). We traced the boundaries between quartz and feldspar in the sample from a thin section photo onto paper and then made a black-and-white image of this tracing (Fig. 7b). We then estimated the areal proportions of quartz and feldspar from the image with a surface-integrating graphic program (NIH-Image 1.6). In equating areal proportions with volume proportions of quartz and feldspar in the

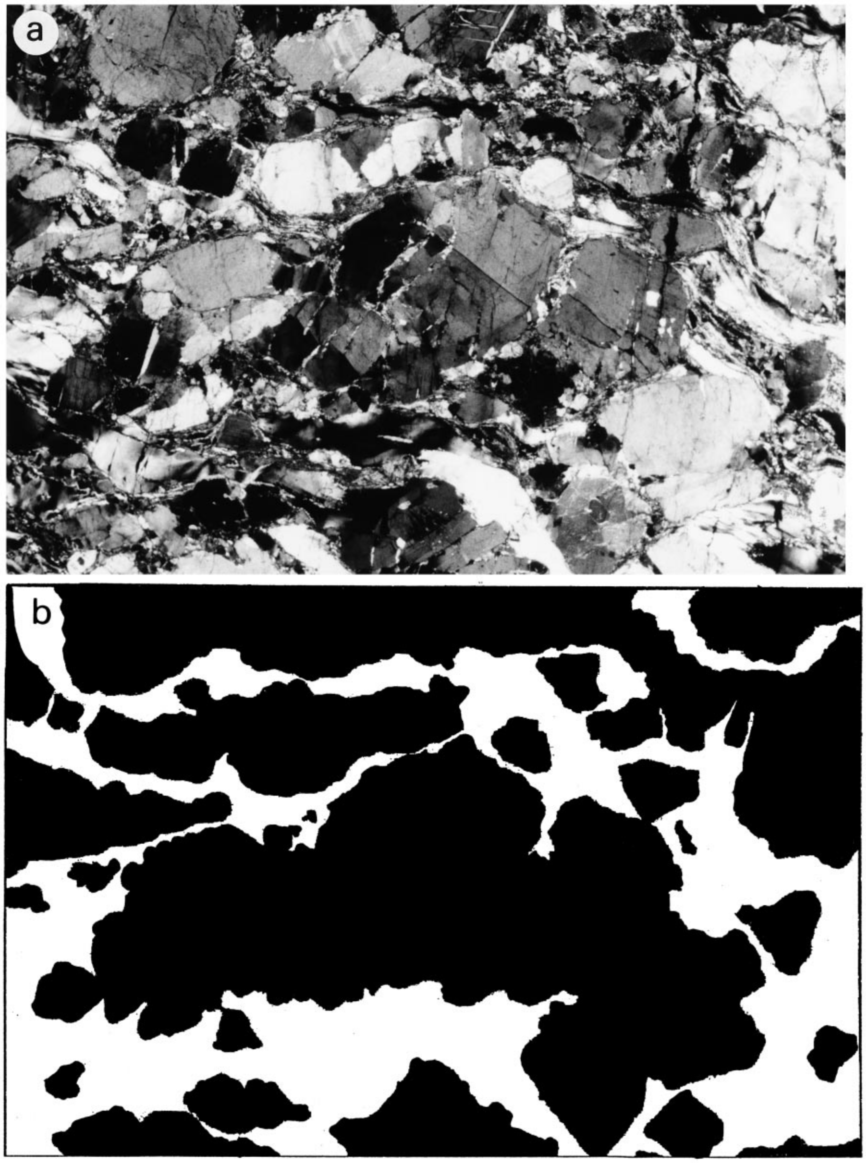

Fig. 7. (a) Micrograph of a greenschist facies, granitoid clastomylonite containing 28 vol.% quartz and 72 vol.% feldspar. (b) Black-and-white image of the mylonite shown in (a) used to calculate areal proportions (see text for explanation); q = quartz, f = feldspar. Photo length is 3 cm, sample number HD-47.

sample, we neglected the slicing or truncation effect (e.g., Exner, 1972). This is justified in light of the complicated phase geometries and probably results in only a slight underestimate of the actual volume proportions of feldspar in the rock.

Depending on the assumed shear strain rate, the shear strength of the quartz–feldspar clastomylonite is predicted to have ranged from 220 to 515 MPa for $T = 350$ºC and 420 to 475 MPa for $T = 400$ºC (Fig. 8). These values are about 2 to 20 times higher than flow stress estimates for quartzite mylonites (20–150 MPa) obtained with dynamically recrystallized grain-size palaeopiezometers (Etheridge and Wilkie, 1981). This discrepancy may be insignifi-

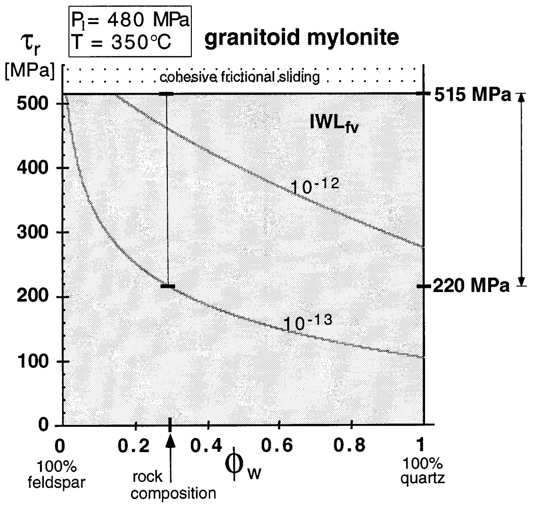

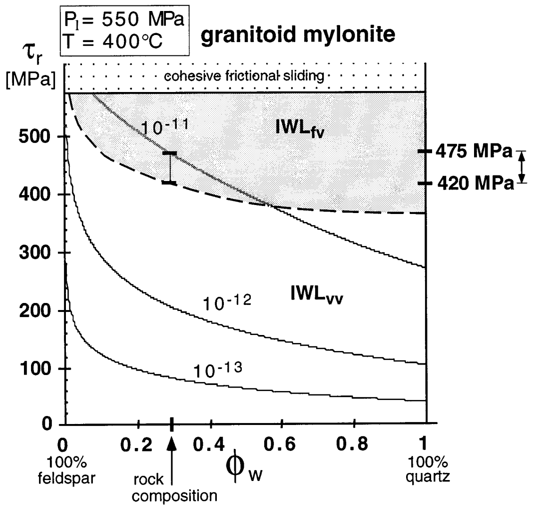

Fig. 8. Shear strength versus bimineralic composition diagrams with shear strength contours (thick lines) and isopleths (thin lines) for the greenschist facies, granitoid clastomylonite described in the text and depicted in Fig. 7. Arrows indicate range of estimated shear strengths. Thick dashed line in lower diagram delimits IWL_{fv} and IWL_{vv} stability fields. Experimental flow parameters for quartz and feldspar as in Fig. 3. Diagrams constructed with equations discussed in text and the flow laws of Jaoul et al. (1984) for quartzite, Shelton and Tullis (1981) for albitic feldspar rock, and the constants of Byerlee (1978) for cohesive frictional sliding (material parameters listed in caption to Fig. 3).

cant given the many analytical and theoretical uncertainties of both our method and the grain-size palaeopiezometers. Nevertheless, the higher strength estimates for quartz–feldspar mylonite are reasonable, insomuch as feldspathic aggregates have higher laboratory strengths than quartzite at the same temperature (Carter and Tsenn, 1987; Kohlstedt et al., 1995) and feldspar clasts in quartz–feldspar mylonite are known to concentrate stress in the interconnected quartz layers (Handy, 1990). Our relatively higher strength estimate compared to that for mylonitic quartzite is also qualitatively consistent with the finding of Hansen and Carter (1982) that the creep exponent and activation energy of power law creep for dry granite is higher than that for quartzite at the same laboratory conditions of deformation. Unfortunately, a better test of our method for estimating the strength of clastomylonites is not yet possible, because there are currently no published experimental flow laws for a bimineralic rock and its two constituent minerals, all determined at the same conditions of temperature, strain rate, confining pressure and pore fluid pressure.

We point out that the method above for estimating bulk strength should really only be applied to mylonitic rocks in which there is no microstructural evidence of significant diffusive mass transfer between the mineral phases that accommodate most of the deformation (e.g., during pressure-solution creep or diffusion-accommodated grain-boundary sliding). Diffusive mass transfer mechanisms are strongly grain-size-sensitive, relax intragranular stresses (White, 1976) and are usually associated with changes in the volume proportions of the constituent phases (Wheeler, 1987). The latter condition violates the basic assumption made in the approach above that the volume proportions of both phases do not vary with strain. Generally, grain-size-sensitive creep mechanisms are associated with lower viscous strengths than grain-size-insensitive, power law creep. Therefore, if our method were applied to rocks in which diffusive massive transfer in the matrix was the dominant, strain-accommodating process, it would probably overestimate the actual strength of the rock.

4. Discussion and conclusions

Consideration of combined frictional and viscous rheologies in mylonite has several implications, first for the terminology of fault rocks and deformational processes, and second for the rheological interpretation of natural fault rocks at the transition from frictional to viscous deformation in the lithosphere. Our model of bimineralic, FV mylonitic flow indicates that the rheology of clastomylonites is strongly dependent on temperature, strain rate, and mineral volume proportion, with only a modest pressure sensitivity due to brittle, dilatational deformation of the porphyroclasts. Even small amounts of a weak mineral ($\phi_w < 0.1$) suffice for the weak mineral to govern the rheology of the whole rock. This is intuitively reasonable in light of the observation that most of the strain in mylonites with an IWL microstructure is accommodated within a weak mineral undergoing dynamic recrystallization and/or diffusion-accommodated grain-boundary sliding (Handy, 1990). Thus, the widespread use of the term 'semibrittle' to describe the rheology both of clastomylonites and of cataclastic fault rocks undergoing adhesive wear (e.g., Scholz, 1988) is somewhat misleading from a mechanistic standpoint, as the behaviour of clastomylonites is predominantly nonlinear viscous.

The prediction above that shear strength within the depth range of FV mylonitic flow decreases with increasing depth and temperature (Fig. 3) is only partly consistent with Scholz's synoptic model of strength and microstructure within the transitional domain between fully frictional sliding (abrasive wear) at shallow depths and fully viscous flow deep in the crust (Scholz, 1988, 1990). Scholz (1988) argues that adhesive wear mechanisms (e.g., intracrystalline plasticity in asperities on fault surfaces) can engender mylonitic fabrics and microstructure, even though the overall behaviour of the fault rock is frictional. In his concept, the presence of mylonitic fault rock at depth signifies the temperature-dependent onset of intracrystalline plasticity (see his fig. 4). We propose that the onset of intracrystalline plasticity in quartz does not correspond with the development of mylonite, because at low temperatures such plasticity involves dislocation glide on an insufficient number of slip systems (usually only one or two) to accommodate large strains compatibly. This is expected to lead to work-hardening followed by brittle failure and cataclasis after only small strains. Schmid and Handy (1990) point out that two conditions are necessary for mylonite to form: (1) Thermally activated dislocation climb must be possible in at least one of the minerals of the rock to prevent that phase from hardening and to allow this phase to accommodate large strains by undergoing dynamic recovery and recrystallization. Deformation studies in both naturally and experimentally deformed, polycrystalline quartzite indicate that relatively small strains ($\gamma < 1$, $e < 10\%$) suffice to initiate dynamic recovery and recrystallization (e.g., ; White, 1976, 1979; Weathers et al., 1979; Dell'Angelo and Tullis, 1989; Hirth and Tullis, 1992). (2) The weak phase must form interconnected layers subparallel to the shearing plane, i.e., the rock must have an IWL microstructure. Reviewing the literature on experimentally deformed two-phase materials, Handy (1994a) cites coaxial strains of about 10–30% for the brittle breakdown of an LBF microstructure to form an IWL microstructure. Both of these conditions are fulfilled only after a critical amount of strain has accrued. It follows that the transition from cataclastic to mylonitic deformation, as well as the depth of the shear strength maximum within the lithosphere are strain- and composition-dependent features.

The generic strength versus depth profiles for granitic crust in Fig. 9 summarize some new and modified notions on crustal rheology stemming from our study of combined frictional and viscous rheologies in clastomylonite. The most obvious modification is that FV mylonitic flow occupies a depth interval between cohesive frictional flow involving adhesive wear and fully viscous mylonitic flow (compare configurations A and B in Fig. 9). In all rocks (except those with very small ϕ_w values), the crustal strength maximum is expected to coincide with the upper depth limit of FV mylonitic flow (see also Sibson, 1983, his fig. 2). This is where temperatures are sufficiently high to facilitate dislocation creep (i.e., dislocation glide-plus-climb) in the weakest mineral of the rock, enabling an IWL_{fv} microstructure to form with schistosity subparallel to the shearing plane. The value of the strength maximum at the intersection of the strength curves for cohesive frictional flow and FV mylonitic flow is less than that obtained if one were only to consider a direct change from cohesive frictional flow to fully viscous flow in mylonite with an IWL_{vv}, microstructure (compare peak strengths for configurations A and B in Fig. 9).

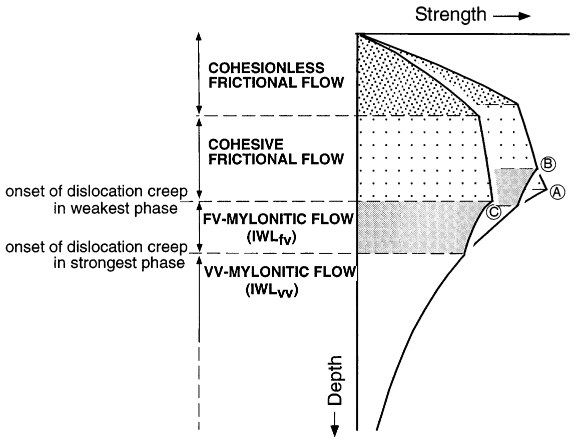

Fig. 9. Synoptic shear strength versus depth profile through granitic crust showing relationship between crustal strength, type of steady-state flow and microstructure, and dominant deformation mechanisms (see text for discussion). Patterned depth intervals are same as in Fig. 3. Three configurations of strength curves depicting strength maxima for the following mechanistic and microstructural transitions (see text): A = direct transition from cohesive frictional flow to fully viscous mylonitic flow with an $\mathrm{IWL_{vv}}$ microstructure; B = transition from cohesive frictional flow to FV mylonitic flow at zero pore fluid pressure; C = transition as in B but at high pore fluid pressure.

High pore fluid pressures considered in the previous section ($\lambda_v = 0.9$, Fig. 6) expand the depth range of FV mylonitic flow, and both decrease and depress the crustal strength maximum (and with it, the upper depth limit of mylonitization) to greater depths (compare configurations B and C in Fig. 9).

Although cataclastic flow mechanisms have been treated only summarily in this paper, we included bulk shear strength curves in Fig. 9 for stable frictional flow in the upper crust. The kink in the strength curve for frictional flow marks changes in the values of cohesion, τ_o, and frictional coefficient, μ_d, on active faults. These changes may be related to the onset of one or more creep processes (e.g., pressure-solution, dislocation glide, Stesky et al., 1974) that also cement fragments and/or weld asperities on sliding surfaces. Thus, our model accounts at least in principle for fault compaction and lithification which can lead to the build-up of near-lithostatic pore fluid pressures. Such pore fluid pressures can significantly reduce frictional fault strength, as recently modelled by Streit (1997). The consideration of near-lithostatic pore fluid pressures (configuration 3 in Fig. 9) allows us to predict peak flow strengths for bimineralic rocks that are comparable to flow stress estimates from quartz grain-size palaeopiezometers applied to natural quartz-rich mylonites.

As mentioned in previous work (Handy, 1994a), deformation mechanisms other than dislocation creep and frictional sliding (e.g., granular flow accommodated by diffusion and/or by the syntectonic nucleation and growth of new mineral phases, Stünitz and FitzGerald, 1993) are associated with different composite flow laws than the ones employed in this paper (Fueten and Robin, 1992; Wheeler, 1992). Characterizing and modelling such deformational processes will modify the view of lithospheric rheology presented here, particularly as regards rocks that deform at or near the limits of their mineralogical stability.

Acknowledgements

We thank Claudio Rosenberg, Andreas Schlaefke, Susanne Palm and Peter Bauer for discussions. G. Mitra and especially S.M. Schmid provided critical reviews that helped us avoid semantic pitfalls and clarified our presentation and argumentation. The computer program used to calculate Figs. 3, 4, 6 and 8 was written in Mathematica 2.2™ by S. Wissing as part of her diploma thesis. Copies of this program are available on request from the first two authors. The support of the Deutsche Forschungsgemeinschaft in the form of DFG- Grant Ha 2403/1-1 is acknowledged with gratitude.

References

Atkinson, B.K., 1984. Subcritical crack growth in geological materials. J. Geophys. Res. 89 (B6), 4077–4114.

Atkinson, B.K., Meridith, P.G., 1987. The theory of subcritical crack growth with applications to minerals and rocks. In: Atkinson, B.K. (Ed.). Fracture Mechanics of Rock. Academic Press, London, pp. 111– 166.

Boland, J.N., Tullis, T.E., 1986. Deformation behaviour of wet and dry clinopyroxene in the brittle to ductile transition region. In: Hobbs, B.E., Heard, H.C. (Eds.), Mineral and Rock Deformation: Laboratory Studies (The Paterson Volume). Am. Geophys. Union, Geophys. Monogr. 36, 35–50.

Byerlee, J., 1978. Friction of rocks. Pure Appl. Geophys. 116, 615–626.

Carter, N.L., Kirby, S.H., 1978. Transient creep and semibrittle behavior of crystalline rocks. Pure Appl. Geophys. 116, 807–839.

Carter, N.L., Tsenn, M.C., 1987. Flow properties of continental lithosphere. Tectonophysics 136, 27–63.

Chopra, P.N., Paterson, M.S., 1981. The experimental deformation of dunite. Tectonophysics 78, 453–473.

Dell'Angelo, L.N., Tullis, J., 1989. Fabric development in experimentally sheared quartzites. Tectonophysics 169, 1–21.

Etheridge, M.A., 1983. Differential stress magnitudes during regional deformation and metamorphism: upper bound imposed by tensile fracturing. Geology 11, 232–234.

Etheridge, M.A., Wilkie, J.C., 1981. An assessment of dynamically recrystallized grainsize as a paleopiezometer in quartz-bearing mylonite zones. Tectonophysics 78, 475–508.

Evans, B., Kohlstedt, D.L., 1995. Rheology of rocks. In: Rock Physics and Phase Relations: A Handbook of Physical Constants. Am. Geophys. Union, Reference Shelf 3, 148–165.

Exner, H.E., 1972. Analysis of grain- and particle-size distributions in metallic materials. Int. Metall. Rev. 17, 25–42.

Fueten, F., Robin, P.Y.-F., 1992. Finite element modelling of a pressure solution cleavage seam. J. Struct. Geol. 14, 953–962.

Handin, J., 1966. Strength and ductility. In: Clark, S.P. (Ed.), Handbook of Physical Constants. Geol. Soc. Am. Mem. 97, 223–289.

Handin, J., Hager Jr., R.V., Friedman, M., Feather, J.N., 1963. Experimental deformation of sedimentary rocks under confining pressure: pore pressure tests. Am. Assoc. Pet. Geol. Bull. 47, 718–755.

Handy, M.R., 1987. The structure, age, and kinematics of the Pogallo fault zone, Southern Alps, northwestern Italy. Eclogae Geol. Helv. 80 (3), 593–632.

Handy, M.R., 1990. The solid-state flow of polymineralic rocks. J. Geophys. Res. 96 (B6), 8647–8661.

Handy, M.R., 1994a. Flow laws for rocks containing two non-linear viscous phases: a phenomenological approach. J. Struct. Geol. 16 (3), 287–301.

Handy, M.R., 1994b. Correction to 'Flow laws for rocks containing two nonlinear viscous phases: a phenomenological approach'. J. Struct. Geol. 16 (12), 1727.

Hansen, F.D., Carter, N.L., 1982. Creep of selected crustal rocks at 1000 MPa. Eos 63, 437.

Hirth, G., Tullis, J., 1992. Dislocation creep regimes in quartz aggregates. J. Struct. Geol. 14, 145–160.

Ivins, E.R., Sammis, C.G., 1996. Transient creep of a composite lower crust, 1. Constitutive theory. J. Geophys. Res. 101 (B12), 27981–28004.

Jaeger, J.C., Cook, N.G.W., 1979. Fundamentals of Rock Mechanics, 3rd Edition. Chapman and Hall, London, 583 pp.

Jaoul, O., Tullis, J., Kronenberg, A.K., 1984. The effect of varying water contents on the creep behaviour of Heavitree Quartzite. J. Geophys. Res. 89 (B6), 4281–4287.

Ji, S., Zhao, P., 1993. Flow laws of multiphase rocks calculated from experimental data on the constituent phases. Earth Planet. Sci. Lett. 117, 181–187.

Ji, S., Zhao, P., 1994. Strength of two-phase rocks: a model based on fiber-loading theory. J. Struct. Geol. 2, 253–262.

Kohlstedt, D.L., Weathers, M.S., 1980. Deformation-induced microstructures, paleopiezometers and differential stresses in deeply eroded fault zones. J. Geophys. Res. 85 (B11), 6269–6285.

Kohlstedt, D.L., Evans, B., Mackwell, S.J., 1995. Strength of the lithosphere: constraints imposed by laboratory experiments. J. Geophys. Res. 100 (B9), 17587–17602.

Mitra, G., 1978. Ductile deformation zones and mylonites: the mechanical processes involved in the deformation of crystalline basement rocks. Am. J. Sci. 278, 1057–1084.

Mitra, G., 1984. Brittle to ductile transition due to large strains along the White Rock thrust, Wind River mountains, Wyoming. J. Struct. Geol. 6, 51–61.

Murrel, S.A.F., 1965. The effect of triaxial stress systems on the strength of rocks at atmospheric temperatures. J. Geophys. R. Astron. Soc. 10, 231–281.

Nye, J.F., 1953. The flow law of ice from measurements in glacier tunnels, laboratory experiments and the Jungfraufim borehole experiment. Proc. R. Soc. London 219, 477–489.

Ord, A., Christie, J.M., 1984. Flow stresses from microstructures in mylonitic quartzites of the Moine Thrust Zone, Assynt area, Scotland. J. Struct. Geol. 6 (6), 639–654.

Paterson, M.S., 1978. Experimental Rock Deformation — The Brittle Field. Springer, Berlin, 254 pp.

Paterson, M.S., 1987. Problems in the extrapolation of laboratory rheological data. Tectonophysics 133, 33–43.

Schmid, S.M., Handy, M.R., 1990. Towards a genetic classification of fault rocks: geological usage and tectonophysical implications. In: Hsii, K.J., Mackenzie, J., Mtiller, D. (Eds.), Controversies in Modern Geology. Academic Press, London, pp. 339–362.

Scholz, C.H., 1988. The brittle–plastic transition and the depth of seismic faulting. Geol. Rundsch. 77 (1), 319–328.

Scholz, C.H., 1990. The Mechanics of Earthquakes and Faulting. Cambridge University Press, Cambridge, 439 pp.

Secor, D.T., 1965. Role of fluid pressure in jointing. Am. J. Sci. 263, 633–646.

Shelton, G., Tullis, J., 1981. Experimental flow laws for crustal rocks. Eos 62 (17), 396.

Sibson, R.H., 1977. Fault rocks and fault mechanisms. J. Geol. Soc. London 133, 191–213.

Sibson, R.H., 1981. Controls on low-stress hydro-fracture dilatancy in thrust, wrench and normal fault terrains. Nature 289, 655–657.

Sibson, R.H., 1983. Continental fault structure and the shallow earthquake source. J. Geol. Soc., London 140, 741–767.

Sibson, R.H., 1986. Earthquakes and rock deformation in crustal fault zones. Annu. Rev. Earth Planet. Sci. 14, 149–175.

Sibson, R.H., 1994. Crustal stress, faulting and fluid flow. In: Parnell, J. (Ed.), Geofluids: Origin, Migration and Evolution of Fluids in Sedimentary Basins. Geol. Soc. Spec. Publ. 78, pp. 69–84.

Stesky, R.M., Brace, W.F., Riley, D.R., Robin, P.-Y., 1974. Friction in faulted rock at high temperature and pressure. Tectonophysics 23, 177–203.

Streit, J.E., 1997. Low frictional strength of upper crustal faults: a model. J. Geophys. Res. 102, 24619–24626.

Streit, J.E., Cox, S.F., 1998. Fluid infiltration and volume change during midcrustal mylonitization of Proterozoic granite, King Island, Tasmania. J. Metamorph. Geol. 16, 197–212.

Stünitz, H., FitzGerald, J.D., 1993. Deformation of granitoids at low metamorphic grade, II. Granular flow in albite-rich mylonites. Tectonophysics 221, 299–324.

Tullis, T.E., Horowitz, F.G., Tullis, J., 1991. Flow laws of polyphase aggregates from end-member flow laws. J. Geophys. Res. 96 (B5), 8081–8096.

Weathers, M., Bird, J., Cooper, R.F., Kohlstedt, D.L., 1979. Differential stress determined from deformation-induced microstructures of the Maine Thrust Zone. J. Geophys. Res. 84 (B13), 7495–7509.

Weertman, J., 1968. Dislocation climb theory of steady state creep. Trans. Am. Soc. Metals 61, 681–694.

Wheeler, J., 1987. The significance of grain-scale stresses in the kinetics of metamorphism. Contrib. Mineral. Petrol. 97, 397–404.

Wheeler, J., 1992. Importance of pressure solution and coble creep in the deformation of polymineralic rocks. J. Geophys. Res. 97 (B4), 4579–4586.

White, S., 1976. The effects of strain on the microstructures, fabrics and deformation mechanisms in quartzites. Philos. Trans. R. Soc. London, A 283, 69–86.

White, S., 1979. Grain and sub-grain size variations across a mylonite zone. Contrib. Mineral. Petrol. 70, 193–202.

White, S.H., Burrows, S.E., Carreras, J., Shaw, N.O., Humphreys, F.J., 1980. On mylonites in ductile shear zones. J. Struct. Geol. 2 (1/2), 175–187.